Corrosion Science 258 (2026) 113323

Contents lists available at ScienceDirect

Corrosion Science

journal homepage: www.elsevier.com/locate/corsci

Estimating standard adsorption Gibbs energy from corrosion inhibition efficiencies: A case of multilayer adsorption

Anton Kokalj

Department of Physical and Organic Chemistry, Jožef Stefan Institute, Jamova 39, SI-1000 Ljubljana, Slovenia

ARTICLE INFO

Keywords:
Multilayer adsorption
Corrosion inhibition
Surface coverage
Adsorption isotherm
Standard adsorption free energy

ABSTRACT

In corrosion inhibition studies, the standard adsorption Gibbs energy is often estimated from c/θ versus c plots, where c is the inhibitor concentration and θ is the surface coverage. In doing so, inhibition efficiency (η) is assumed to be a good approximation of surface coverage, i.e., $\theta \approx \eta$. Consequently, adsorption is effectively treated as monolayer adsorption, since inhibition efficiency is, by definition, confined to values below one. However, there is no fundamental physical reason why adsorption on flat surfaces should be limited to a monolayer. For this reason, a model that maps multilayer surface coverage to inhibition efficiency is developed based on a few reasonable physical assumptions. It is shown that multilayer adsorption reduces the slope of the c/η versus c curve — widely interpreted as the c/θ curve due to the $\theta \approx \eta$ approximation — and leads to a more pronounced curvature compared to the monolayer case. While the bending at low concentrations resembles that caused by repulsive lateral interactions, the overall curvature remains a distinct feature of multilayer adsorption. However, it is argued that in experiments — where only a limited number of data points are typically obtained — these features are often not distinctive enough to allow multilayer identification. This helps explain why the $\theta \approx \eta$ approximation, which implicitly assumes monolayer adsorption, has been so widely accepted and used.

1. Introduction

In many corrosion inhibition studies, inhibition efficiency (η) is commonly used as a proxy for fractional surface coverage (θ), i.e., $\theta \approx \eta$. The standard adsorption Gibbs energy ($\Delta G^{\circ}_{\mathrm{ads}}$) is then estimated from the relation $c/\theta = 1/K + nc$, where c is the inhibitor concentration in the bulk solution, K is the adsorption equilibrium constant, and n is the slope of the c/θ line. This linear relation was shown in previous work [1] — the first paper in this series — to be an effective approach for estimating $\Delta G^{\circ}_{\mathrm{ads}}$ in a variety of monolayer adsorption scenarios, including systems with lateral interactions, multisite adsorption, and surface heterogeneities. The relation originates from the Langmuir adsorption isotherm, in which the slope is $n = 1$. Experimental studies frequently report a linear dependence of c/θ on c, although the slope often deviates significantly from unity. As shown in the first paper [1], such deviations signal non-Langmuir adsorption behavior: repulsive lateral interactions, multisite adsorption, and surface heterogeneities lead to slopes greater than one, while attractive interactions result in slopes below one.

In the second paper [2], a new monolayer adsorption isotherm was proposed to improve the estimation of the standard adsorption Gibbs energy. This isotherm, derived from an analysis of the c/θ versus c behavior across different monolayer adsorption models, was shown to be sufficiently flexible to describe a wide range of monolayer adsorption scenarios.

In the third paper [3], motivated by the observation of Lindsay et al. [4] that the $\theta \approx \eta$ assumption may not always hold, a model was developed to map inhibition efficiency to surface coverage more reliably. This model was validated using experimental data from Lindsay et al. [4].

In all three papers [1–3], monolayer adsorption was assumed. This assumption stems from the $\theta \approx \eta$ approximation, since inhibition efficiency is, by definition, confined to values below one. However, there is no fundamental physical reason why adsorption on flat surfaces should be limited to a monolayer, unless the interactions between molecules are repulsive—a condition that typically arises only between charged species of the same sign. Indeed, multilayer adsorption of inhibitors has been inferred experimentally [5–9] and observed in molecular simulations [10,11].

In this paper, we therefore extend the analysis to multilayer adsorption and investigate its implications for c/η versus c plots. These

E-mail address: tone.kokalj@ijs.si.
URL: http://www.ijs.si/ijsw/K3-en/Kokalj.

https://doi.org/10.1016/j.corsci.2025.113323
Received 31 July 2025; Accepted 17 September 2025
Available online 29 September 2025

plots are widely interpreted as c/θ plots in corrosion inhibition studies due to the common use of the $\theta \approx \eta$ approximation, referred to as the *perfect adsorption hypothesis* in Ref. [12]. The term "perfect" reflects the assumption that an adsorbed molecule perfectly blocks corrosion at its adsorption site.

A natural strategy for addressing this theoretically is to develop a model that maps multilayer surface coverage to inhibition efficiency. Even if such a model is a poor representation of the relationship between adsorption and corrosion inhibition, it may still offer valuable insight. A notable analogy is the Langmuir adsorption model [13], which — despite its simplicity and idealizations — has proven exceptionally useful in adsorption studies. Building on this rationale, the multilayer inhibition efficiency model developed herein is based on the Brunauer–Emmett–Teller (BET) adsorption theory [14]. It extends the monolayer model from the third paper [3] by incorporating the effects of subsequent adsorbate layers on corrosion inhibition through a set of reasonable physical assumptions. This model enables us to examine the influence of multilayer adsorption on c/η versus c plots. It is shown that such plots — although they may exhibit features characteristic of multilayer adsorption — generally do not display sufficiently distinctive signatures to allow reliable multilayer identification in experiments. This helps explain why the $\theta \approx \eta$ approximation — which implicitly assumes monolayer adsorption — has been so widely accepted and used.

This manuscript is structured as follows. In the next Theory section, a model that maps multilayer surface coverage to inhibition efficiency is developed. The subsequent Results and discussion section explores the implications of the multilayer model, and the main findings are summarized in the Conclusions section. This is followed by three appendices: Appendix A concisely summarizes technical details, while Appendices B and C present derivations of the BET and BET-n adsorption isotherms, respectively, in support of the Theory section.

2. Theory

A plausible model, based on a few simple physical assumptions, that links inhibition efficiency with surface coverage for a (sub)monolayer adsorption was developed in a previous work [3]. Herein, we extent the model to a multilayer adsorption.

Before proceeding, let us define some basic quantities. Let S_0, S_1, $S_2\ldots$, S_i stand for surface areas that are exclusively covered by 0, 1, 2…, i layers of adsorbed molecules (Fig. 1a). Hence, the total surface area is:

$$S = \sum_{i=0}^{\infty} S_i, \tag{1}$$

and the fraction of the surface that is exclusively covered by i layers is given by:

$$\theta_i = \frac{S_i}{S}, \tag{2}$$

whereas the fraction of the surface that is covered by at least one molecular layer ($\theta_{1(+)}$) is:

$$\theta_{1(+)} = \sum_{i=1}^{\infty} \theta_i. \tag{3}$$

Eqs. (1) and (2) imply that

$$\sum_{i=0}^{\infty} \theta_i = 1. \tag{4}$$

Hence, from Eqs. (3) and (4), the fraction of the uncovered surface (θ_0) can be written as:

$$\theta_0 = 1 - \theta_{1(+)}. \tag{5}$$

The basic assumption of the multilayer model presented here is that the formation of molecular layers beyond the first does not influence the corrosion protectiveness of the first adsorbed layer. This

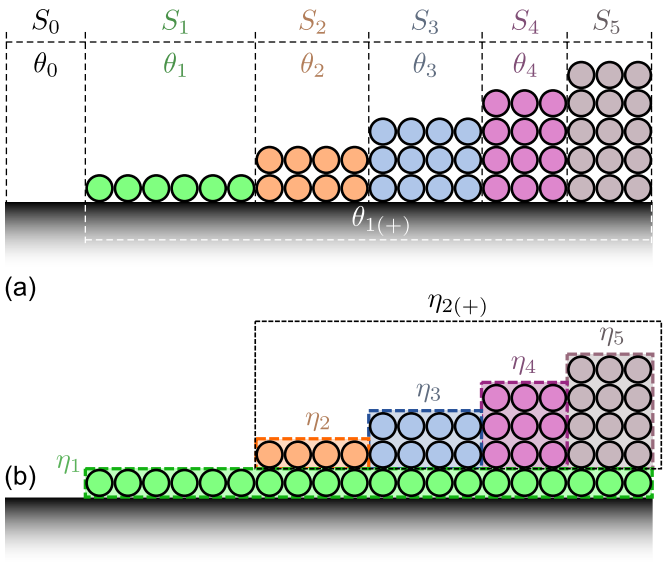

Fig. 1. (a) Schematic definition of surface areas S_0, S_1, $S_2\ldots$ that are exclusively covered by 0, 1, 2… layers of adsorbed molecules, respectively, and the corresponding exclusive relative coverages θ_i. (b) Schematic definition of inhibition efficiency of the first layer (η_1) and of the layers beyond it ($\eta_{2(+)}$). The latter is given by $\sum_{i=2}^{\infty}\eta_i$, where η_i corresponds to the $\eta_{2(+)}$ component of inhibition efficiency due to the fraction of the surface exclusively covered by i layers. In contrast, η_1 corresponds to the fraction of the surface that is covered by at least one molecular layer, i.e., η_1 corresponds to $\theta_{1(+)}$, whereas, for $i \geq 2$, η_i corresponds to θ_i.

assumption appears reasonable because the mechanisms by which the first adsorbate layer and the subsequent layers inhibit corrosion differ. Specifically, chemisorbed inhibitors in the first layer directly retard the cathodic and/or anodic reactions by blocking active surface sites, whereas subsequent inhibitor layers primarily impede mass transport processes [6], for example by acting as a dielectric barrier [15,16]. Hence, the overall inhibition efficiency (η) due to multilayer adsorption can be expressed as the sum of the inhibition efficiency of the first layer (η_1) and the layers beyond it ($\eta_{2(+)}$):

$$\eta = \eta_1 + \eta_{2(+)} = \eta_1 + \sum_{i=2}^{\infty} \eta_i, \tag{6}$$

where η_i corresponds to the $\eta_{2(+)}$ component of inhibition efficiency due to the fraction of the surface exclusively covered by i layers. The η_1 and $\eta_{2(+)}$ components, along with η_i contributions to $\eta_{2(+)}$, are schematically presented in Fig. 1b. The first-layer η_1 can be described by the monolayer model developed in the previous work [3], i.e.:

$$\begin{aligned}\eta_1 &= \eta_1^{\max}(1-(1-\theta_{1(+)})^{m/\eta_1^{\max}}) \\ &= \eta_1^{\max}(1-\theta_0^{m/\eta_1^{\max}}), \qquad \text{where } \eta_1^{\max} \in [0,1).\end{aligned} \tag{7}$$

Here, m denotes the number of surface sites protected by a single inhibitor molecule at very low coverage; it can be less than or greater than 1. The parameter $\eta_1^{\max}$ represents the maximum achievable inhibition efficiency due to first-layer adsorption, corresponding to a surface fully covered by a molecular monolayer. For a more detailed discussion of the model and its derivation, see Ref. [3].

It is worth noting that for $m = \eta_1^{\max}$, Eq. (7) simplifies to:

$$\eta_1 = \eta_1^{\max}(1-\theta_0) = \eta_1^{\max}\theta_{1(+)} \qquad \text{for } m = \eta_1^{\max}, \tag{8}$$

implying that the inhibition efficiency of the first-layer depends linearly on the $\theta_{1(+)}$ coverage with the slope of $\eta_1^{\max}$.

The characteristics of the monolayer model, developed in the previous work [3], are shown in Fig. 2a, which displays the dependence

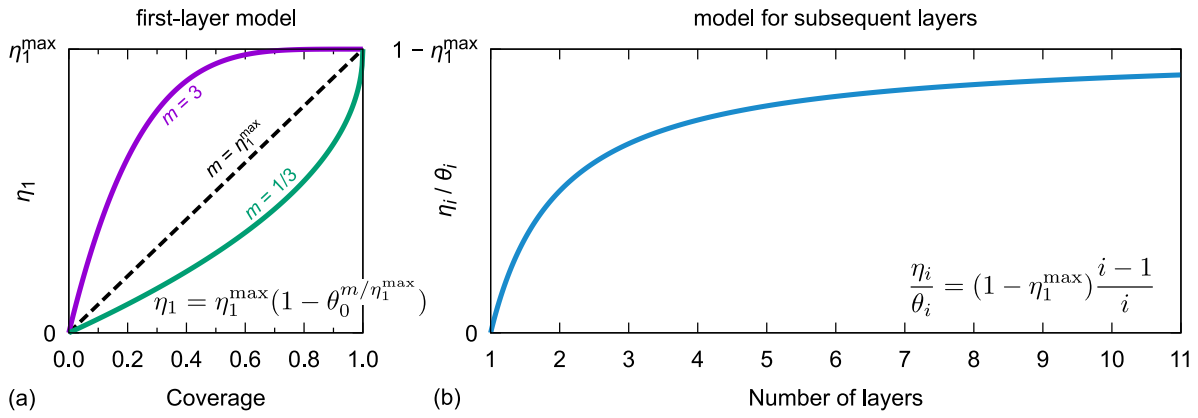

Fig. 2. (a) Dependence of the first-layer inhibition efficiency (η_1) on the fraction of the surface covered by at least one molecular layer ($\theta_{1(+)}$), according to the model of Eq. (7) for $m = 3$ (purple), $m = \eta_1^{max}$ (black dashed), and $m = 1/3$ (green); the graph is plotted with $\eta_1^{max} = 0.7$. (b) For subsequent molecular layers, the dependence of the ith layer inhibition efficiency (η_i) on the number of molecular layers (i) for $\theta_i = 1$, which is equivalent to η_i/θ_i.

of the first-layer inhibition efficiency η_1 on the coverage $\theta_{1(+)}$ for $m = 3, \eta_1^{max}$, and $1/3$. With these choices of m, all three qualitatively different cases are represented: $m = 3$ corresponds to a case where an inhibitor molecule protects more than one site at low coverage; $m = 1/3$ illustrates a case where an inhibitor molecule only partially protects the site it occupies at low coverage; and $m = \eta_1^{max}$ corresponds to the case where η_1 depends linearly on $\theta_{1(+)}$.

To build the model for $\eta_{2(+)}$, we utilize the Brunauer–Emmett–Teller (BET) multilayer adsorption model [14,17] — a short derivation of the BET isotherm is presented in Appendix B — and the assumption that $\eta_{2(+)}$ smoothly increases with coverage, such that total inhibition efficiency η asymptotically approaches unity as the coverage goes to infinity. This is a reasonable assumption because when the sample is covered by an infinitely-thick inhibitor multilayer, it is not exposed to a corrosive environment. Hence, corrosion should stop. Therefore, the boundary conditions for $\eta_{2(+)}$ are:

$$\begin{aligned} &\text{for } \theta = 0: \quad \eta_{2(+)} = 0, \\ &\text{for } \theta = \infty: \quad \eta_{2(+)} = 1 - \eta_1^{max} \quad \text{and} \quad \partial\eta_{2(+)}/\partial\theta = 0. \end{aligned} \tag{9}$$

These boundary conditions can be fulfilled, if η_i, introduced in Eq. (6), is written as:

$$\eta_i = (1-\eta_1^{max})\frac{i-1}{i}\theta_i. \tag{10}$$

So defined η_i consists of three components:

- $(1-\eta_1^{max}) \equiv$ the maximum value of $\eta_{2(+)}$,
- $\frac{i-1}{i} \equiv$ the protectiveness of the i layers,
- $\theta_i \equiv$ the fraction of the surface exclusively covered by the i layers.

Note that the expression $(i-1)/i$ has the same algebraic structure as the Langmuir isotherm, $\theta = Kc/(1+Kc)$. By substituting Kc with $i-1$, one obtains $(i-1)/i$. As the coverage goes to infinity, the number of layers above the surface approaches infinity; hence, $i \to \infty$ and $(i-1)/i \to 1$. The dependence of η_i/θ_i — which can be seen as η_i for $\theta_i = 1$ — on i is presented in Fig. 2b. From Eqs. (6) and (10), $\eta_{2(+)}$ can be written as:

$$\eta_{2(+)} = (1-\eta_1^{max})\sum_{i=2}^{\infty}\frac{i-1}{i}\theta_i. \tag{11}$$

2.1. The BET multilayer model

In the BET multilayer adsorption model, θ_i is given by Eq. (B.15) in Appendix B:

$$\theta_i = w\theta_0 x^i. \tag{12}$$

Inserting this expression into Eq. (11), we obtain:

$$\begin{aligned} \eta_{2(+)} &= (1-\eta_1^{max})\, w\theta_0 \sum_{i=2}^{\infty}\frac{i-1}{i}x^i \\ &= (1-\eta_1^{max})\, w\theta_0 \left(\ln(1-x) + \frac{x}{1-x}\right) \qquad \text{for } x < 1, \end{aligned} \tag{13}$$

where:

$$x = cK_2, \tag{14}$$

$$w = \frac{K_1}{K_2}, \tag{15}$$

$$\theta_0 = \frac{1-x}{1-x+wx} \qquad \text{for } x < 1. \tag{16}$$

Here, c is the concentration of the inhibitor in the bulk solution, K_1 is the adsorption equilibrium constant for adsorption on bare surface (i.e., for first-layer adsorption), and K_2 is the adsorption equilibrium constant for adsorption on molecular layers (i.e., for adsorption beyond the first layer).

By plugging the expression for θ_0 of Eq. (16) into Eq. (13), the equation can be rewritten as:

$$\eta_{2(+)} = (1-\eta_1^{max})\, w\, \frac{(1-x)\ln(1-x)+x}{1-x+wx} \qquad \text{for } x < 1. \tag{17}$$

A convenient feature of expressing the protectiveness component of $\eta_{2(+)}$ as $(i-1)/i$ is that the sum in Eq. (13) can be written in closed form:

$$\sum_{i=2}^{\infty}\frac{i-1}{i}x^i = \ln(1-x) + \frac{x}{1-x} \qquad \text{for } x < 1. \tag{18}$$

Note that the $\ln(1-x)$ term diverges at $x = 1$, and becomes complex-valued for $x > 1$. Physically, $x = 1$ marks the onset of molecular condensation on the surface, which, mathematically, corresponds to an infinitely thick multilayer. The concentration at which this occurs is denoted by c_{cond} and is given by (cf. Eq. (14)):

$$c_{cond} = \frac{1}{K_2}. \tag{19}$$

To obtain a workable expression for $\eta_{2(+)}$ at any concentration, it is necessary to guard against this divergence. This can be achieved by recognizing that once the coverage becomes mathematically *infinite* at c_{cond}, it remains *infinite* at concentrations exceeding c_{cond}. The first step toward obtaining a workable expression is to replace $1-x$ with the function:

$$t(x) = \begin{cases} 1-x & \text{for } x < 1, \\ 0 & \text{for } x \geq 1. \end{cases} \tag{20}$$

The second step is to observe that:

$$\lim_{x\to 1}(1-x)\ln(1-x) = 0, \tag{21}$$

which justifies replacing $(1-x)\ln(1-x)$ with the function:

$$L(x) = \begin{cases} (1-x)\ln(1-x) & \text{for } x < 1, \\ 0 & \text{for } x \geq 1. \end{cases} \tag{22}$$

Correspondingly, the expression for $\eta_{2(+)}$ of Eq. (17) can be rewritten as:

$$\eta_{2(+)} = (1-\eta_1^{\max})\, w\, \frac{L(x)+x}{t(x)+wx}. \tag{23}$$

The full expression for inhibition efficiency can now be obtained by combining Eqs. (6), (7), (16), (20), (22), and (23):

$$\eta = \eta_1^{\max}\left(1-\left(\frac{t(x)}{t(x)+wx}\right)^{m/\eta_1^{\max}}\right) + (1-\eta_1^{\max})\, w\, \frac{L(x)+x}{t(x)+wx}. \tag{24}$$

It is worth noting that in the limit $x \to 1$ with $t(x) \to 0$ and $L(x) \to 0$, η tends to 1, i.e.:

$$\begin{aligned} \lim_{x\to 1}\eta &= \eta_1^{\max}\left(1-\left(\frac{\cancelto{0}{t(x)}}{\cancelto{0}{t(x)}+wx}\right)^{m/\eta_1^{\max}}\right) + (1-\eta_1^{\max})\, w\, \frac{\cancelto{0}{L(x)}+x}{\cancelto{0}{t(x)}+wx} \\ &= \eta_1^{\max} + (1-\eta_1^{\max}) w \frac{x}{wx} = 1, \end{aligned} \tag{25}$$

which reflects the built-in assumption of the model that an infinitely thick inhibitor layer fully suppresses corrosion. This limit also confirms that the divergence-free expression for $\eta_{2(+)}$, given by Eq. (23), is consistent and correctly formulated.

2.2. The BET-*n* multilayer model

For the BET-*n* multilayer model (see Appendix C), which considers at most n adsorbate layers, the derivation is analogous to that of the BET model ($n = \infty$), except that the summations are evaluated only up to n terms. In this case, Eq. (13) becomes:

$$\eta_{2(+)}(n) = (1-\eta_1^{\max})\, w\, \theta_0(n) \sum_{i=2}^{n} \frac{i-1}{i} x^i, \tag{26}$$

where $\theta_0(n)$ denotes the fraction of uncovered surface, as defined in Eq. (C.2), and is analogous to θ_0 in the standard BET model. However, this summation cannot be written in a simple closed form and must be evaluated explicitly. Hence:

$$\eta_{2(+)}(n) = (1-\eta_1^{\max})\, w \left(1 + w\frac{x(1-x^n)}{1-x}\right)^{-1} \sum_{i=2}^{n} \frac{i-1}{i} x^i. \tag{27}$$

In contrast, the expression for η_1 is analogous to Eq. (7), but with θ_0 replaced by $\theta_0(n)$, i.e.:

$$\eta_1(n) = \eta_1^{\max}\left(1-\theta_0(n)^{m/\eta_1^{\max}}\right). \tag{28}$$

The full expression for the inhibition efficiency in the BET-*n* model is thus given by:

$$\eta(n) = \eta_1(n) + \eta_{2(+)}(n). \tag{29}$$

The maximum inhibition efficiency achievable by the BET-*n* model is less than one, as at most n adsorbate layers can form. It is given by:

$$\eta^{\max}(n) = \lim_{x\to\infty} \eta(n) = \eta_1^{\max} + (1-\eta_1^{\max})\frac{n-1}{n}. \tag{30}$$

3. Results and discussion

The multilayer models developed above are characterized below using several examples. The BET-based model depends on two parameters and two constants: (i) m, the number of surface sites protected by a single inhibitor molecule at very low coverage; (ii) $\eta_1^{\max}$, the maximum achievable inhibition efficiency from first-layer adsorption; (iii) K_1, the equilibrium constant for adsorption on the bare surface; and (iv) K_2, the equilibrium adsorption constant for subsequent layers. In addition, the BET-*n*-based model also depends on n, the maximum number of layers an adsorbate can form.

The adsorption equilibrium constants are calculated from the standard adsorption Gibbs energies ($\Delta G^{\circ}_{\text{ads}}$), which are more intuitive to use than the equilibrium constants themselves. As is commonly done, inhibitor adsorption is considered as substitutional adsorption:

$$\text{Mol}_{(\text{sol})} + \text{H}_2\text{O}_{(\text{ad})} \rightleftharpoons \text{Mol}_{(\text{ad})} + \text{H}_2\text{O}_{(\text{sol})}, \tag{31}$$

where Mol denotes the inhibitor molecule, and the subscripts (sol) and (ad) refer to a solvated molecule in the bulk solution and an adsorbed molecule, respectively. For this reaction, the equilibrium adsorption constant is calculated as follows [1]:

$$K = \frac{1}{c_{\text{H}_2\text{O}}} \exp\left(-\frac{\Delta G^{\circ}_{\text{ads}}}{RT}\right), \tag{32}$$

where $c_{\text{H}_2\text{O}}$ is the molar concentration of liquid water (55.34 M at 25 °C). Note that in the BET multilayer adsorption model, two adsorption constants are used: K_1 for the bare surface and K_2 for the molecular layers above it.

If, instead, the inhibitor adsorption is treated as plain adsorption, $\text{Mol}_{(\text{sol})} \rightleftharpoons \text{Mol}_{(\text{ad})}$, the corresponding equilibrium constant is given by [1]:

$$K = \frac{1}{c^{\circ}} \exp\left(-\frac{\Delta G^{\circ\,\text{plain}}_{\text{ads}}}{RT}\right), \tag{33}$$

where the standard-state concentration is typically taken as $c^{\circ} = 1$ M. By equating Eqs. (32) and (33), the standard adsorption Gibbs energies for plain and substitutional adsorption are related as follows:

$$\Delta G^{\circ\,\text{plain}}_{\text{ads}} = \Delta G^{\circ}_{\text{ads}} + 10\ \text{kJ/mol} \qquad \text{at } T = 298.15\ \text{K}. \tag{34}$$

For the analysis, a relatively low value of $\eta_1^{\max}$ of 0.7 is purposely chosen to emphasize the effect of the multilayer adsorption on the inhibition efficiency. In analogy with Fig. 2a, three representative values of m — namely 3, $\eta_1^{\max}$, and 1/3 — are considered to capture all qualitatively distinct cases: a case where an inhibitor molecule protects more than one site at low coverage ($m = 3$); a case where an inhibitor molecule only partially protects the site it occupies at low coverage ($m = 1/3$); and a case where η_1 depends linearly on $\theta_{1(+)}$ ($m = \eta_1^{\max}$). As for standard adsorption Gibbs energies, $\Delta G^{\circ}_{1,\text{ads}} = -30$ kJ/mol is used for adsorption on bare surface, and $\Delta G^{\circ}_{2,\text{ads}} = -20$ kJ/mol is used for adsorption on the subsequent molecular layers; the corresponding values of K_1 and K_2 are 3027 and 54.91 M^{-1}.

The value of $\Delta G^{\circ}_{1,\text{ads}} = -30$ kJ/mol was chosen for two reasons. First, it falls within the order of magnitude of many $\Delta G^{\circ}_{\text{ads}}$ values reported in the corrosion inhibition literature. Second, it lies between the commonly cited threshold values of −20 and −40 kJ/mol, which are often used to distinguish between physisorption and chemisorption—hence the choice of −20 kJ/mol for $\Delta G^{\circ}_{2,\text{ads}}$. However, this 20/40 criterion was recently criticized [18] for being an unreliable means of distinguishing between the two adsorption modes.

3.1. Dependence of surface coverage and inhibition efficiency on concentration

Fig. 3a shows the dependence of coverage and inhibition efficiency on inhibitor concentration for the BET adsorption isotherm and the multilayer inhibition-efficiency model of Eq. (24), respectively. Fig. 3b displays the corresponding relations for the BET-10 model (i.e., the BET-*n* model with $n = 10$). At low inhibitor concentrations, adsorption on the bare surface dominates as indicated by $\theta \approx \theta_{1(+)}$, and the inhibition efficiency increases rapidly—the greater the value of m, the faster the increase. Once adsorption on the bare surface builds a monolayer to a sufficient extent — for the considered values of $\Delta G^{\circ}_{1,\text{ads}}$ and $\Delta G^{\circ}_{2,\text{ads}}$, this occurs at $\theta_{1(+)} \approx 0.7$ — adsorption on subsequent layers begins. As a result, the coverage quickly exceeds one and continues to

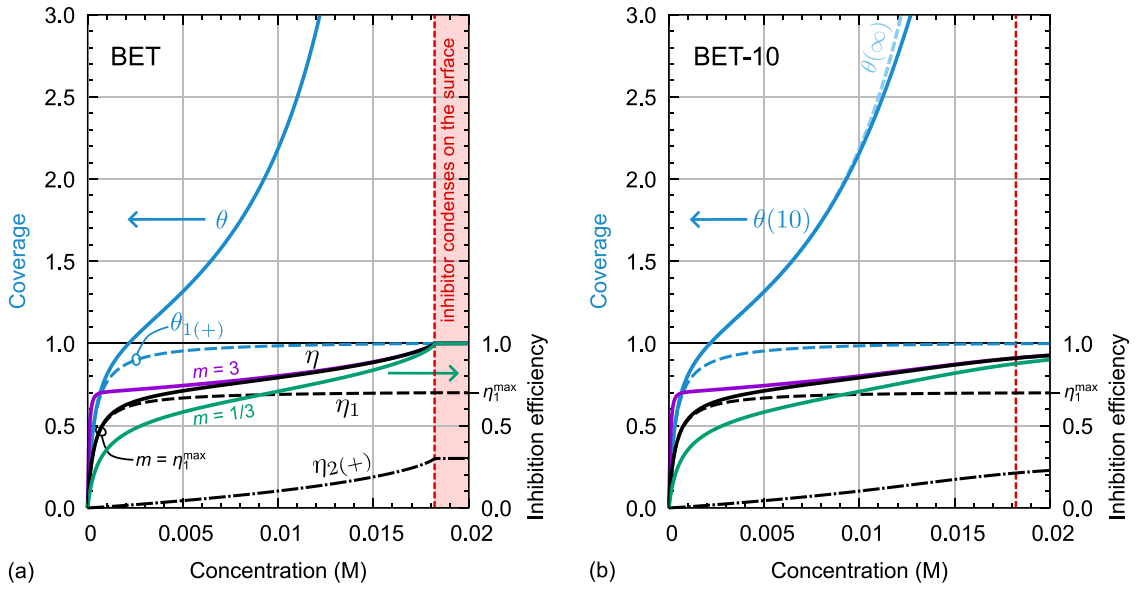

Fig. 3. Dependence of inhibitor surface coverage (blue) and inhibition efficiency — shown for $m = 3$ (purple), $m = \eta_1^{\max}$ (black), and $m = 1/3$ (green) — on the inhibitor concentration in the bulk solution for (a) the BET model and (b) the BET-n model with $n = 10$ (i.e., BET-10). The curves were calculated using $\Delta G^{\circ}_{1,\mathrm{ads}} = -30$ kJ/mol, $\Delta G^{\circ}_{2,\mathrm{ads}} = -20$ kJ/mol, and $\eta_1^{\max} = 0.7$. The η_1 and $\eta_{2(+)}$ components of the inhibition efficiency are also shown: η_1 is plotted for $m = \eta_1^{\max}$, while $\eta_{2(+)}$ is independent of m. For the BET model, the inhibition efficiency exhibits a discontinuity in slope at the concentration at which the inhibitor condenses on the surface (indicated by the vertical red dashed line), whereas the BET-10 curves are smooth.

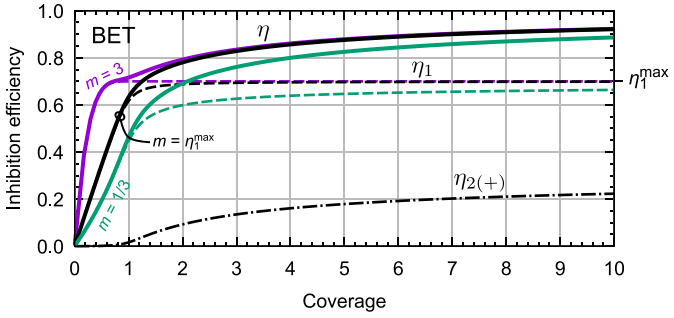

Fig. 4. Dependence of inhibition efficiency (η) on surface coverage for the BET model, shown for $m = 3$ (purple), $m = \eta_1^{\max}$ (black), and $m = 1/3$ (green). The curves were calculated using $\Delta G^{\circ}_{1,\mathrm{ads}} = -30$ kJ/mol, $\Delta G^{\circ}_{2,\mathrm{ads}} = -20$ kJ/mol, and $\eta_1^{\max} = 0.7$. For each m, the first-layer component (η_1) of η is shown by a dashed line in the corresponding color, while the $\eta_{2(+)}$ component, which is independent of m, is shown by a black dash-dotted line.

increase with concentration. However, around this point, the increase in inhibition efficiency becomes slower with increasing concentration. At sufficiently high concentration, condensation of the inhibitor on the surface sets in for the BET model—for the current value of $\Delta G^{\circ}_{2,\mathrm{ads}}$, this occurs at $c = 18.2$ mM (indicated by the red vertical dashed line). At this point, the inhibition efficiency curves for the BET model exhibit a discontinuity in slope, and the efficiency reaches a value of one, reflecting the built-in assumption of the model that an infinitely thick inhibitor layer fully suppresses corrosion. In contrast, the BET-10 model does not exhibit a discontinuity in slope, and its inhibition efficiency remains below one.

An alternative representation of Fig. 3 is provided by Fig. 4, which shows the dependence of inhibition efficiency on coverage for the BET model. This figure more clearly reveals that inhibition efficiency increases rapidly during the buildup of the first monolayer, whereas for subsequent layers, the increase becomes more gradual. The figure also shows that the $\eta_{2(+)}$ component of inhibition efficiency begins to build up when $\theta \gtrsim 1$.

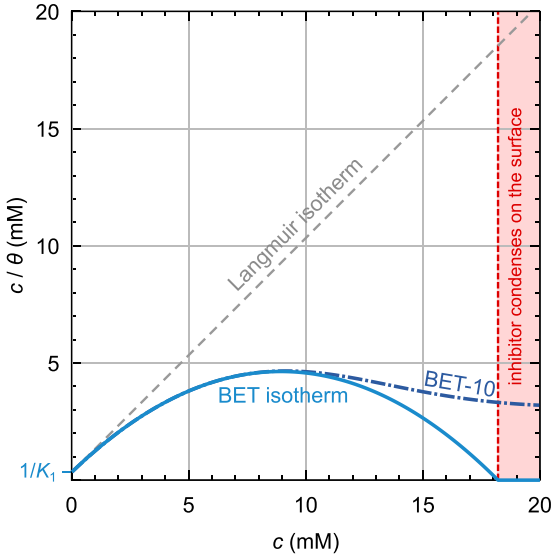

Fig. 5. Plot of c/θ versus c for the BET, BET-10, and Langmuir isotherms. Curves were computed using $\Delta G^{\circ}_{1,\mathrm{ads}} = -30$ kJ/mol and $\Delta G^{\circ}_{2,\mathrm{ads}} = -20$ kJ/mol. The concentration c_{cond}, at which inhibitor condensation on the surface occurs in the BET model, is indicated by the vertical red dashed line. Note the discontinuity in the slope of the BET curve at this point.

3.2. c/θ and c/η dependence on concentration

In corrosion inhibition studies, the standard adsorption Gibbs energy is commonly estimated from a c/θ versus c plot. However, this approach relies on the assumption $\eta \approx \theta$, which does not hold in the case of multilayer adsorption, since $\eta \leq 1$ while θ can exceed unity (cf. Fig. 3). This observation implies that, in practice, $\Delta G^{\circ}_{\mathrm{ads}}$ is instead estimated from the c/η versus c plot.

Fig. 5 presents the BET, BET-10, and Langmuir adsorption isotherms on a c/θ versus c plot. At low concentrations, both BET isotherms follow

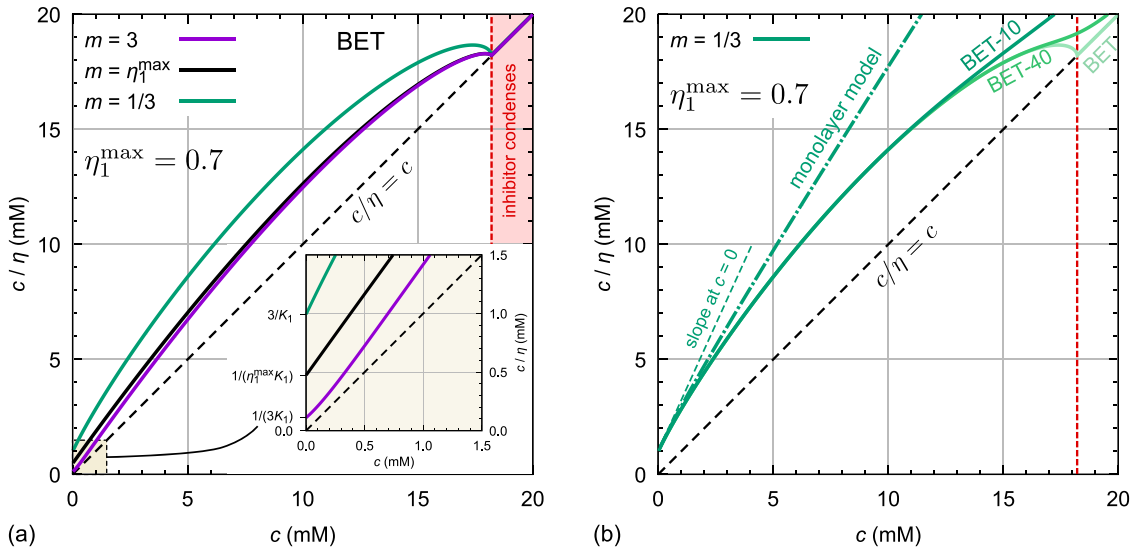

Fig. 6. (a) Plot of c/η versus c for the BET model, shown for $m = 1/3$ (green), $m = \eta_1^{\max}$ (black), and $m = 3$ (purple). (b) Comparison of the monolayer model of Eq. (40) with the multilayer BET-10, BET-40, and BET models. All curves were calculated using $\Delta G^{\circ}_{1,\mathrm{ads}} = -30$ kJ/mol, $\Delta G^{\circ}_{2,\mathrm{ads}} = -20$ kJ/mol, and $\eta_1^{\max} = 0.7$. The black dashed line represents the relation $c/\eta = c$, while the inset in (a) shows the curves at low concentrations to reveal the corresponding intercepts at $c = 0$. Inhibitor condensation on the surface occurs at the concentration indicated by the vertical red dashed line; note the discontinuities in slope exhibited by the BET curves at this point.

the Langmuir isotherm, which, in this form, is given by:

$$\frac{c}{\theta} = \frac{1}{K_1} + c. \tag{35}$$

The Langmuir isotherm thus has a slope of 1 and an intercept of K_1^{-1}. The BET isotherm, expressed in the $c/\theta = f(c)$ form (cf. Eq. (B.20)), is given by:

$$\frac{c}{\theta} = \frac{1}{K_1}(1 - cK_2)(1 - cK_2 + cK_1) \qquad \text{for } c \le \frac{1}{K_2}, \tag{36}$$

implying that it is quadratic in c over the range $c \in [0, K_2^{-1}]$. Above the concentration $c_{\mathrm{cond}} = K_2^{-1}$, the coverage remains infinite, yielding $c/\theta = 0$. A more appropriate form of Eq. (36) is therefore:

$$\frac{c}{\theta} = \begin{cases} \dfrac{1}{K_1}(1 - cK_2)(1 - cK_2 + cK_1) & \text{for } c \le K_2^{-1}, \\ 0 & \text{otherwise.} \end{cases} \tag{37}$$

For the considered example, with $K_1 = 3027\ \mathrm{M}^{-1}$ and $K_2 = 54.91\ \mathrm{M}^{-1}$, we have $K_1 \gg K_2$, and $cK_2 \to 0$ at low c, so that the BET isotherm reduces to the Langmuir form in this limit. As the concentration increases, the coverage grows, and the slope of the BET isotherm gradually decreases, reaching zero at a maximum located at $c = 8.9$ mM. It can be shown that this maximum occurs at:

$$c = \frac{K_1 - 2K_2}{2K_2(K_1 - K_2)}. \tag{38}$$

Beyond this point, the slope becomes negative, and the c/θ curve reaches zero at $c_{\mathrm{cond}} = 18.2$ mM, where inhibitor condensation at the surface begins and the BET coverage diverges to infinity. In contrast, the BET-10 isotherm does not exhibit a discontinuity at c_{cond}. After reaching a local maximum at approximately 9 mM, its slope becomes negative. However, as shown in Fig. S1 in the Supplementary material, the slope eventually begins to increase again and approaches a value of 1/10 as $c \to \infty$, since in this limit $\theta = 10$ for the BET-10 model.

While Fig. 5 illustrates the c/θ dependence on c for the exemplar cases of BET and BET-10 multilayer adsorption, it is not practically useful because, in practice, $\Delta G^{\circ}_{\mathrm{ads}}$ is instead estimated from the c/η versus c plot due to the $\theta \approx \eta$ approximation. Hence, we now turn to the c/η dependence on c, which is shown in Fig. 6a, where the BET model of Eq. (24), developed in the Theory section is utilized. In addition to the K_1 and K_2 constants, utilized in Fig. 5, this model depends also on the $\eta_1^{\max}$ and m parameters.

The resulting curves in Fig. 6a resemble the BET parabola in Fig. 5, but are geometrically transformed to lie along the $c/\eta = c$ line instead of the abscissa. Note that the lower the value of m, the more pronounced the curvature of the resulting curve. Indeed, the curves with $m \ge \eta_1^{\max}$ lie closer together, as illustrated by the purple and black curves in Fig. 6a. In contrast, the curvature becomes more pronounced for $m < \eta_1^{\max}$, with the curves arching more noticeably above the $c/\eta = c$ line. Hence, the slope of the curves appear greater than one at low concentrations, which is shown below to result primarily from $\eta_1^{\max} < 1$, rather than from multilayer adsorption.

To scrutinize the effect of multilayer adsorption on the number of adsorbed layers — and to distinguish it from monolayer adsorption in the c/η versus c plots — Fig. 6b compares the BET multilayer model with the BET-40, BET-10, and monolayer models, using $m = 1/3$ and $\eta_1^{\max} = 0.7$. For the monolayer model, the Langmuir isotherm is considered, and the coverage is calculated as:

$$\theta_{\mathrm{L}} = \frac{cK_1}{1 + cK_1}, \tag{39}$$

where the subscript L denotes the coverage calculated using the Langmuir isotherm. The inhibition efficiency is then calculated analogously to Eq. (7) as:

$$\eta_1 = \eta_1^{\max}(1 - (1 - \theta_{\mathrm{L}})^{m/\eta_1^{\max}}). \tag{40}$$

In agreement with Fig. 5, Fig. 6b shows that at low concentrations, all the considered models yield the same results, as monolayer adsorption dominates. However, as the concentration increases, the BET and BET-n curves begin to bend below that of the monolayer model, with their slopes decreasing progressively. For the BET curve, the slope eventually becomes negative, and at c_{cond} it touches the $c/\eta = c$ line and follows it thereafter. Based on numerical analysis, it can be conjectured that the slope from the left approaches $-\infty$ at c_{cond}, as a consequence of the divergence of the BET model at this concentration. In contrast to the BET curve, the BET-n curves do not exhibit a discontinuity in slope at c_{cond}. The figure further reveals that the larger the value of n, the longer the BET-n curve follows the BET curve—e.g., the BET-10 curve follows the BET curve up to approximately $c = 13$ mM, whereas the BET-40 curve follows it up to about $c = 17$ mM. At concentrations above

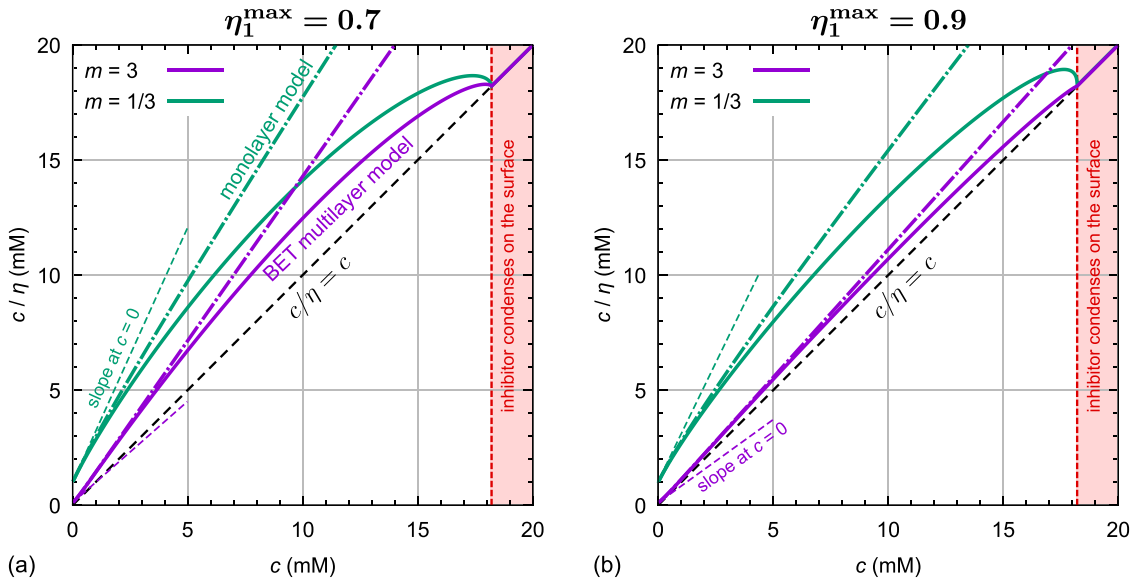

Fig. 7. Comparison of the BET multilayer model of Eq. (24) (solid curves) with the monolayer model of Eq. (40) (dash-dotted) on c/η versus c plots for $m = 1/3$ (green) and $m = 3$ (purple), with (a) $\eta_1^{max} = 0.7$ and (b) $\eta_1^{max} = 0.9$. The curves were calculated using $\Delta G^{\circ}_{1,ads} = -30$ kJ/mol and $\Delta G^{\circ}_{2,ads} = -20$ kJ/mol. The slopes at $c = 0$ are indicated by thin dashed lines in the corresponding colors.

c_{cond}, the BET-n curve asymptotically approaches the $c/\eta^{max}(n)$ line, where $\eta^{max}(n)$ is given by Eq. (30). These observations suggest that as n increases from 1 to ∞, the monolayer curve gradually transforms into the BET curve, as schematically illustrated Fig. S2 in the Supplementary material.

To scrutinize the effect of the η_1^{max} parameter on the shape and slope of the c/η curves, Fig. 7 compares the BET multilayer model with the monolayer model at $\eta_1^{max} = 0.7$ and 0.9, for $m = 1/3$ and 3. The curves at $\eta_1^{max} = 0.7$ are more bent above the $c/\eta = c$ line and, consequently, are steeper at low concentrations than those at $\eta_1^{max} = 0.9$, suggesting that the slope at $c = 0$ increases as η_1^{max} decreases. This trend was analytically confirmed in previous work [3] for the monolayer model of Eq. (40), where the asymptotic behavior of c/η was derived in the limits $c \to 0$ and $c \to \infty$:

$$\frac{c}{\eta} = \frac{1}{mK} + \frac{m + \eta_1^{max}}{2m\eta_1^{max}} c \qquad \text{as } c \to 0, \tag{41}$$

and

$$\frac{c}{\eta} \propto \frac{c}{\eta_1^{max}} \qquad \text{for the Langmuir-based model as } c \to \infty. \tag{42}$$

Based on Eq. (41), the intercept and slope at $c = 0$ are thus given by:

$$\text{intercept} = \frac{1}{mK}, \qquad \text{slope} = \frac{m + \eta_1^{max}}{2m\eta_1^{max}}. \tag{43}$$

The $(mK)^{-1}$ intercepts are shown graphically in the inset of Fig. 6a, whereas the slopes at $c = 0$ are indicated by thin dashed lines of the corresponding color in Figs. 6b and 7. Note that the slope at $c = 0$ is less than one for the $m = 3$ curves, although it quickly rises above one as c increases. To provide further insight into the slope at $c = 0$, Fig. S3 in the Supplementary material illustrates its dependence on the parameters m and η_1^{max}. As can be seen, the slope increases as η_1^{max} and m decrease. Furthermore, for $m < 1$, the slope is always greater than one, whereas for $m > 1$, it becomes less than one when $m > \eta_1^{max}/(2\eta_1^{max} - 1)$, provided that $\eta_1^{max} > 0.5$.

Above, we analyzed the dependence of the c/η curves on the parameters m and η_1^{max}, while keeping $\Delta G^{\circ}_{1,ads}$ and $\Delta G^{\circ}_{2,ads}$ constant. We now examine how the shape of the curve depends on the ratio between $\Delta G^{\circ}_{1,ads}$ and $\Delta G^{\circ}_{2,ads}$. To this end, we fix $\Delta G^{\circ}_{1,ads}$ at −30 kJ/mol and vary $\Delta G^{\circ}_{2,ads}$. Fig. 8 shows the curves for $\Delta G^{\circ}_{2,ads} = -20$, −22, and −24 kJ/mol, using $m = 1/3$ and $\eta_1^{max} = 0.7$. The curves exhibit a similar overall shape,

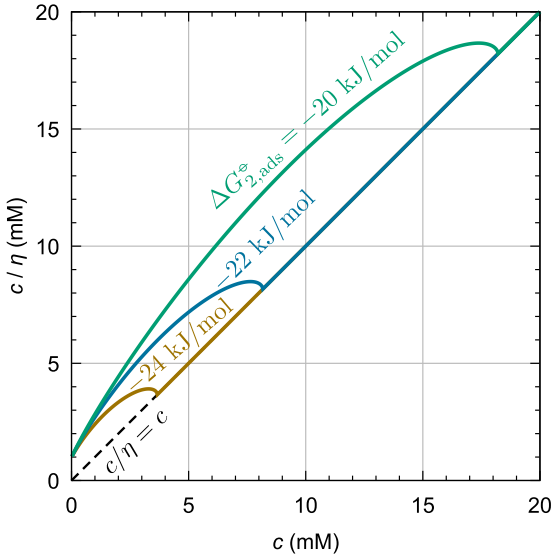

Fig. 8. Dependence of the c/η versus c curves on the ratio between $\Delta G^{\circ}_{1,ads}$ and $\Delta G^{\circ}_{2,ads}$ for the BET multilayer model, using $m = 1/3$ and $\eta_1^{max} = 0.7$. $\Delta G^{\circ}_{1,ads}$ is fixed at −30 kJ/mol, while $\Delta G^{\circ}_{2,ads}$ is set to −20, −22, and −24 kJ/mol.

but the bent, arching portion is progressively compressed toward lower values of c_{cond}, namely 18.2, 8.2, and 3.7 mM, respectively.

Let us conclude this subsection by noting that Figs. 5, 6b, and 7 clearly show that multilayer adsorption reduces the slope of the c/θ and c/η curves compared to monolayer adsorption.

3.3. Benchmarking the multilayer model

Based on the understanding developed above of how multilayer adsorption affects inhibition efficiency, let us now discuss its potential implications for experiments, particularly when plotting experimental data in the c/η versus c form. Before engaging in this analysis, we need to realize the following two important points.

Table 1
Summary of the results of the two virtual experiments described in the main text. $\Delta G_{\text{ads}}^{\text{target}}$ denotes the reference (target) $\Delta G_{\text{ads}}^{\text{fit}}$ values, while $\Delta G_{\text{ads}}^{\text{kokalj}}$ and $\Delta G_{\text{ads}}^{\text{lin}}$ represent the standard adsorption Gibbs energies obtained by fitting the data points using Eqs. (48) and (47), respectively. Values shown in parentheses correspond to the respective standard adsorption Gibbs energies corrected with Eq. (49).

m	$\eta_1^{\max}$	$\Delta G_{\text{ads}}^{\text{target}}$ (kJ/mol)	Experiment–1		Experiment–2	
			$\Delta G_{\text{ads}}^{\text{kokalj}}$ (kJ/mol)	$\Delta G_{\text{ads}}^{\text{lin}}$ (kJ/mol)	$\Delta G_{\text{ads}}^{\text{kokalj}}$ (kJ/mol)	$\Delta G_{\text{ads}}^{\text{lin}}$ (kJ/mol)
1/3	0.7	−27.3 (−30.0)	−27.2 (−29.9)	−24.6 (−27.3)	−27.3 (−30.0)	−27.1 (−29.8)
	0.9		−26.9 (−29.6)	−25.1 (−27.8)	−27.3 (−30.0)	−27.1 (−29.8)
3	0.7	−32.7 (−30.0)	−35.0 (−32.3)	−27.2 (−24.4)	−32.6 (−29.9)	−34.4 (−31.7)
	0.9		−38.2 (−35.4)	−30.5 (−27.8)	−32.8 (−30.0)	−34.0 (−31.3)

1. At low coverage, monolayer adsorption dominates, and the multilayer adsorption system effectively behaves like a monolayer one, provided that $\Delta G^{\circ}_{1,\text{ads}}$ is more exergonic than $\Delta G^{\circ}_{2,\text{ads}}$.
2. In the c/η versus c plots, the effect of multilayer adsorption is small when the value of $\eta_1^{\max}$ approaches one. In this case, the inhibition efficiency is primarily determined by the first adsorbed molecular layer, and the system again behaves effectively as a monolayer one. This observation implies that the significance of multilayer effects increases as $\eta_1^{\max}$ decreases.

Hence, it is worth making some analysis to scrutinize at which inhibitor concentration, the multilayer effects become important. It is much simpler to do such analysis in terms of coverage than inhibition efficiency, so we follow the coverage route.

Let us define the concentration c_{err} as the point at which the coverage $\theta_{1(+)}$ deviates from full coverage θ by a fraction ϵ, such that the two coverages are related by:

$$\theta_{1(+)} = (1-\epsilon)\theta \tag{44}$$

The BET expression for θ is given by Eq. (B.20), whereas the expression for $\theta_{1(+)}$ can be obtained from Eq. (B.17) as:

$$\theta_{1(+)} = 1 - \theta_0 = \frac{cK_1}{1 - cK_2 + cK_1}. \tag{45}$$

By plugging Eqs. (45) and (B.20) into Eq. (44) and solving for c, we obtain a simple expression:

$$c_{\text{err}} = \frac{\epsilon}{K_2} = \epsilon c_{\text{cond}}, \tag{46}$$

where c_{cond} is the concentration at which the inhibitor condenses on the surface, as given by Eq. (19).

Let us arbitrarily set the acceptable error to 10%, i.e., $\epsilon = 0.1$. For the examples presented in Fig. 7, with $\Delta G^{\circ}_{2,\text{ads}} = -20$ kJ/mol, the resulting c_{err} concentration is 1.8 mM. So, at concentration greater than this, the two coverages will deviate by more than 10%, expecting that the multilayer effects will become noticeable. In particular, for the $m = 1/3$ examples (green curves in Fig. 7), the discrepancy in c/η between the monolayer and BET models is calculated to be 6% for $\eta_1^{\max} = 0.7$ and 4% for $\eta_1^{\max} = 0.9$

The above analysis implies that if experiments are performed at concentrations lower than c_{err}, the influence of multilayer effects will be negligible. Conversely, if experiments include concentrations significantly higher than c_{err}, multilayer effects may play a role. However, we show below that even in this latter case, the experimental c/η plots do not clearly reveal the presence of multilayer adsorption.

To this end, we perform two virtual experiments—one at high concentrations up to about c_{cond} and the other at low concentrations ($c \lesssim c_{\text{err}}$). The specific concentrations are as follows:

(i) Experiment–1: $c = 1, 4, 7, 10, 13,$ and 16 mM,
(ii) Experiment–2: $c = 0.1, 0.2, 0.4, 0.8,$ and 1.6 mM.

The equilibrium constants K_1 and K_2 used in these virtual experiments are those introduced in the preceding subsections, derived from $\Delta G^{\circ}_{1,\text{ads}} = -30$ kJ/mol and $\Delta G^{\circ}_{2,\text{ads}} = -20$ kJ/mol. The BET multilayer model of Eq. (24) is employed to generate the $(c, c/\eta)$ data points at the above concentrations, using four different combinations of the parameters m and $\eta_1^{\max}$, namely: $m = 1/3$ and 3; and $\eta_1^{\max} = 0.7$ and 0.9. The dependence of inhibition efficiency on inhibitor concentration for these parameters is plotted in Fig. S4 in the Supplementary material, which shows that inhibition efficiency increases smoothly from 0 to nearly 1 over the concentration range of experiment–1.

The so-generated data points are then fitted with the linear ansatz:

$$\frac{c}{\eta} = \frac{1}{K_{\text{fit}}^{\text{lin}}} + nc, \tag{47}$$

which was shown to be an effective equation that can decently fit various monolayer adsorption models [1]. The respective equilibrium constant is denoted as $K_{\text{fit}}^{\text{lin}}$, where the superscript "lin" indicates the equation used for fitting. The data points are also fitted with the recently introduced Kokalj isotherm [2], which was specifically devised to provide a more accurate fit:

$$\frac{c}{\eta} = \frac{1}{K_{\text{fit}}^{\text{kokalj}}} + nc + c_1\left[\exp\left(-\frac{c}{c_2}\right) - 1\right], \tag{48}$$

where n, c_1, and c_2 are empirical parameters. The resulting adsorption Gibbs energies deduced from $K_{\text{fit}}^{\text{lin}}$ and $K_{\text{fit}}^{\text{kokalj}}$ — denoted as $\Delta G_{\text{ads}}^{\text{lin}}$ and $\Delta G_{\text{ads}}^{\text{kokalj}}$, respectively — are summarized in Table 1 for the two virtual experiments, whereas several representative c/η versus c plots are shown in Fig. 9. Their interpretation is provided after the next paragraph.

Note that when $(c, c/\eta)$ data points are fitted instead of $(c, c/\theta)$ data points, as is currently done, the resulting K_{fit} corresponds to the equilibrium adsorption constant only when $\eta = \theta$. If instead $\eta \neq \theta$, and the relation between the two can be approximated by either Eq. (7) or Eq. (24), then, according to Eq. (43), the intercept at $c = 0$ equals $(mK)^{-1}$, and the relation between the fitted adsorption Gibbs energy ($\Delta G_{\text{ads}}^{\text{fit}}$) and the standard adsorption Gibbs energy is [3]:

$$\Delta G^{\circ}_{\text{ads}} = \Delta G_{\text{ads}}^{\text{fit}} + RT \ln m, \tag{49}$$

implying that the fitted $\Delta G_{\text{ads}}^{\text{fit}}$ can be corrected to obtain a better estimate of the standard adsorption Gibbs energy. However, such a correction can be made only if the parameter m can be deduced from experiments. This requires that the coverage be accurately estimated experimentally by some means for at least one or preferably a few concentrations at which the η values were also measured [3].

The results of the two virtual experiments, presented in Fig. 9, show that the c/η dependence on c ranges from slightly curved to almost perfectly linear. The curvature is most apparent in the high-concentration experiment–1 for the low value of $\eta_1^{\max} = 0.7$ (Figs. 9a and 9b). In contrast, for the low-concentration experiment–2, even the most curved case ($m = 1/3$, $\eta_1^{\max} = 0.7$) appears almost perfectly linear (Fig. 9d). Due to this curvature, the Kokalj isotherm usually fits the data points more accurately than the linear ansatz and follows the multilayer adsorption curves closely. Consequently, the resulting standard adsorption Gibbs energies are much closer to the reference value of −30 kJ/mol (see the values in parentheses in Table 1). The

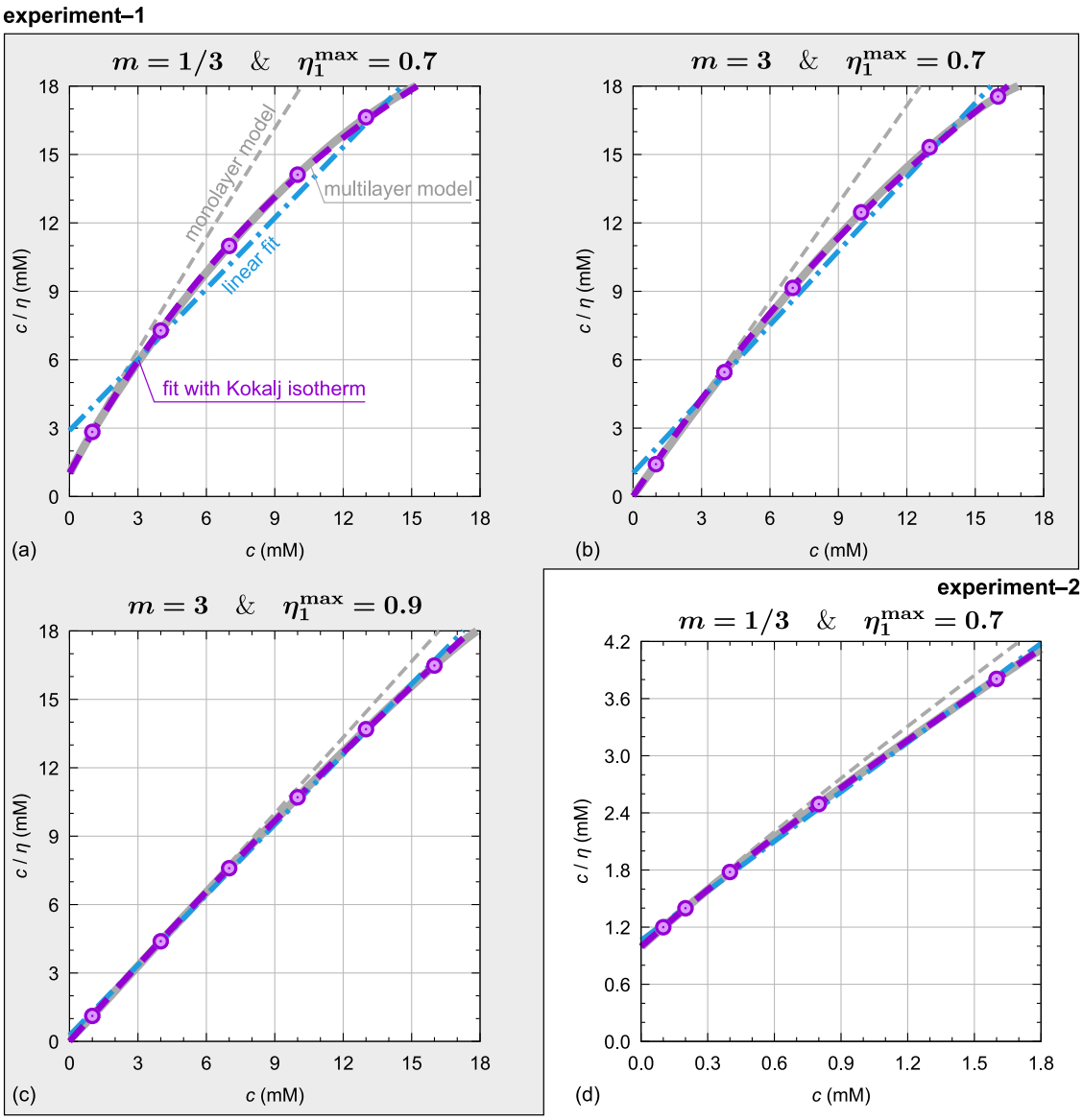

Fig. 9. Representative c/η versus c plots for the two virtual experiments, with data points generated at selected concentrations using the BET multilayer adsorption model of Eq. (24), employing $\Delta G^{\circ}_{1,\mathrm{ads}} = -30$ kJ/mol and $\Delta G^{\circ}_{2,\mathrm{ads}} = -20$ kJ/mol. For each plot, the corresponding m and $\eta_1^{\max}$ values are indicated above it. Gray solid curves show the underlying BET multilayer model; gray dashed curves correspond to the monolayer model of Eq. (40), illustrating the difference between monolayer and multilayer adsorption. Purple dashed curves represent fits based on the Kokalj isotherm of Eq. (48), while blue dash-dotted lines correspond to linear fits using Eq. (47).

linear ansatz is superior only in one case — experiment–1 with $m = 3$ and $\eta_1^{\max} = 0.9$ — which can be attributed to the linearity of the $(c, c/\eta)$ data points (Fig. 9c). Indeed, in the original publication [3], it was pointed out that in nearly linear cases, the Kokalj isotherm may perform poorly because it attempts to fit very small deviations from linearity. As a result, in the limit $c \to 0$, it can become unreasonably curved, leading to an inaccurate estimate of the equilibrium adsorption constant.

These results clearly confirm that when experimental data for multilayer adsorption are fitted in the c/η versus c form, and the equilibrium adsorption constant is estimated from the intercept at $c = 0$, the resulting constant — and thus the standard adsorption Gibbs energy — corresponds to adsorption on the bare surface. This correspondence is not surprising and can be attributed to the $c \to 0$ extrapolation, where monolayer adsorption dominates, provided that $\Delta G^{\circ}_{1,\mathrm{ads}}$ is more exergonic than $\Delta G^{\circ}_{2,\mathrm{ads}}$, which is a typical scenario and the one considered in this work.

While Fig. 9 reveals that, in curved cases, the multilayer model deviates visibly from the monolayer one, the presence of curvature alone is not sufficient to identify multilayer adsorption. Similar curvatures may also arise from repulsive interactions, multisite adsorption, or surface heterogeneities [1]. Thus, additional experimental evidence is required to distinguish multilayer behavior.

These observations support the initial proposition of this work: when inhibition efficiency is used as a proxy for surface coverage, adsorption is effectively treated as monolayer adsorption. This is not only because inhibition efficiency is, by definition, less than one, but also because the resulting c/η versus c dependence — although potentially distinctive according to the present model — is typically represented by a limited number of experimental data points, which are usually insufficient to reliably characterize multilayer adsorption.

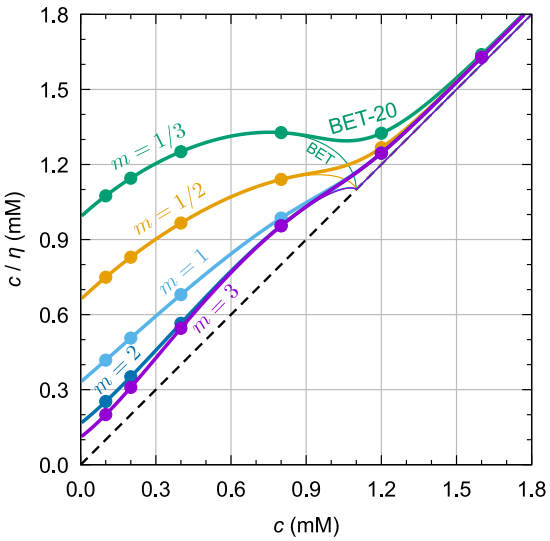

Fig. 10. c/η versus c curves for the BET-20 model, plotted under conditions that emphasize multilayer features. Parameters used are $\Delta G^{\circ}_{1,\mathrm{ads}} = -30$ kJ/mol and $\Delta G^{\circ}_{2,\mathrm{ads}} = -27$ kJ/mol (corresponding to $c_{\mathrm{cond}} = 1.1$ mM), with $\eta_1^{\max} = 0.7$ and $m = 1/3$, 1/2, 1, 2, and 3. Thin curves visible around 1.1 mM correspond to the BET model. Data points are plotted at concentrations of 0.1, 0.2, 0.4, 0.8, 1.2, and 1.6 mM to mimic experimental sampling. For the corresponding η versus c plot, see Fig. S5 in the Supplementary material.

3.4. A quest for multilayer adsorption

Although the c/η versus c curves derived from the present model display some characteristic features of multilayer adsorption, the preceding analysis suggests that these features are generally not recognizable from a limited number of experimental data points. Let us now explore the conditions under which multilayer features become most apparent. A hallmark of the c/η versus c multilayer curve is its bent, arching shape above the $c/\eta = c$ line for $c \le c_{\mathrm{cond}}$, followed by a linear regime beyond this point. In relative terms, this arching becomes more pronounced as the value of $\Delta G^{\circ}_{2,\mathrm{ads}}$ approaches that of $\Delta G^{\circ}_{1,\mathrm{ads}}$. This is a straightforward consequence of curve scaling, as illustrated in Fig. 8, where curves for different $\Delta G^{\circ}_{2,\mathrm{ads}}$ values are compared under otherwise identical conditions.

Fig. 10 presents the case of $\Delta G^{\circ}_{1,\mathrm{ads}} = -30$ kJ/mol and $\Delta G^{\circ}_{2,\mathrm{ads}} = -27$ kJ/mol, with $\eta_1^{\max} = 0.7$ and $m = 1/3$, 1/2, 1, 2, and 3. To better approximate experimental conditions, the BET-20 model is used instead of the BET model to avoid slope discontinuities at c_{cond}. For $\Delta G^{\circ}_{2,\mathrm{ads}} = -27$ kJ/mol, the corresponding value of c_{cond} is 1.1 mM; therefore, the concentration range is chosen from 0 to 1.8 mM to include both the bent and linear segments of the curve, which are necessary to observe the characteristic arching.

The figure reveals that for small values of m (i.e., 1/3 and 1/2), the arching is indeed appreciable, whereas for larger m values, the curvature becomes considerably less pronounced. These observations suggest that multilayer adsorption can be recognized experimentally from c/η versus c plots only in special cases, provided the following conditions are met: (i) $\Delta G^{\circ}_{2,\mathrm{ads}}$ is not too different from $\Delta G^{\circ}_{1,\mathrm{ads}}$, (ii) the m value is small (i.e., $m \lesssim 1/2$), and (iii) the appropriate concentration range is adequately sampled.

3.5. Validation of the model with experimental data

Osman et al. [7] studied polyoxyalkylated maleic anhydride–oleic acid adduct (POAMO-23) as a corrosion inhibitor for mild steel in 1 M H_2SO_4, and interpreted their results as evidence of multilayer adsorption. Their study reports inhibition efficiency at a relatively large number of concentrations, which is essential for distinguishing between monolayer and multilayer adsorption behavior, and therefore offers a valuable opportunity to validate the multilayer model developed in this work. The analysis of their data is presented in Fig. 11.

Fig. 11a shows the concentration dependence of the measured inhibition efficiency. The data were fitted using both the Langmuir-based monolayer model of Eq. (40) and the BET-n-based multilayer model of Eq. (29); for the latter, the BET-8 variant was used, which provides the best fit. Both models yield visually convincing fits to the experimental data; however, the multilayer model more closely follows the data, as further confirmed quantitatively by the coefficients of determination (R^2): 0.996 for the BET-8 compared to 0.959 for the monolayer model.

The corresponding c/η versus c plot in Fig. 11b reveals an almost perfectly linear relationship, with a slope greater than one. This observation aligns with previous findings [1] that the linear ansatz of Eq. (47) can describe a variety of adsorption scenarios reasonably well. Nonetheless, a tiny deviation from linearity appears at concentrations below 0.15 mM. To explore this feature more closely, Fig. 11c zooms into the low-concentration regime. Notably, the plot exhibits a hallmark of multilayer adsorption: an arching curvature below the concentration c_{cond}, followed by a linear regime beyond this point. The position of c_{cond}, as obtained from the multilayer fit, is indicated by the red dashed vertical line.

However, this arching curvature is shallow — and given that the monolayer model also fits the data rather well — the evidence for multilayer adsorption in this case cannot be considered conclusive. Nevertheless, two points are encouraging: (i) the developed multilayer model is able to describe experimental data remarkably well, and (ii) the experimental data show the predicted hallmark shape of the multilayer curve, albeit with a rather shallow curvature.

4. Conclusions

In many corrosion inhibition studies, inhibition efficiency is often taken to be equal to surface coverage. Consequently, adsorption is effectively treated as monolayer adsorption, since inhibition efficiency, by definition, is confined to values below one. However, there is no fundamental physical justification for why adsorption on flat surfaces should be limited to a monolayer.

To investigate the implications of multilayer adsorption for c/η versus c plots — commonly interpreted as c/θ plots due to the widespread use of the $\theta \approx \eta$ approximation — a model was developed that links inhibition efficiency with multilayer surface coverage. This model extends the monolayer framework established in prior work [3], which was validated by experimental results from Ref. [4], by incorporating the contribution of additional adsorbate layers to corrosion inhibition. To this end, the BET adsorption isotherm was adopted to describe multilayer adsorption, while the inhibition efficiency was assumed to asymptotically approach unity as coverage tends to infinity. This assumption appears physically reasonable: when the metal surface is covered by an infinitely thick inhibitor film, exposure to the corrosive medium is effectively eliminated, and corrosion should cease. Although the developed model may not fully capture the complexities of the relationship between adsorption and corrosion inhibition, it still provides useful qualitative insight. A relevant analogy is the Langmuir adsorption model, which — despite its simplicity and idealizations — has proven remarkably useful in adsorption studies.

Both theoretical considerations and the presented virtual experiments demonstrate that when multilayer adsorption data are analyzed using c/η versus c plots, and the adsorption equilibrium constant is estimated from the intercept at $c = 0$, the resulting value — and, consequently, the derived standard adsorption Gibbs energy — corresponds to adsorption on the bare surface. This outcome can be attributed to the $c \to 0$ extrapolation, where monolayer adsorption dominates. It applies provided that $\Delta G^{\circ}_{1,\mathrm{ads}}$ is more exergonic than $\Delta G^{\circ}_{2,\mathrm{ads}}$, which is a typical scenario and the one considered in this work.

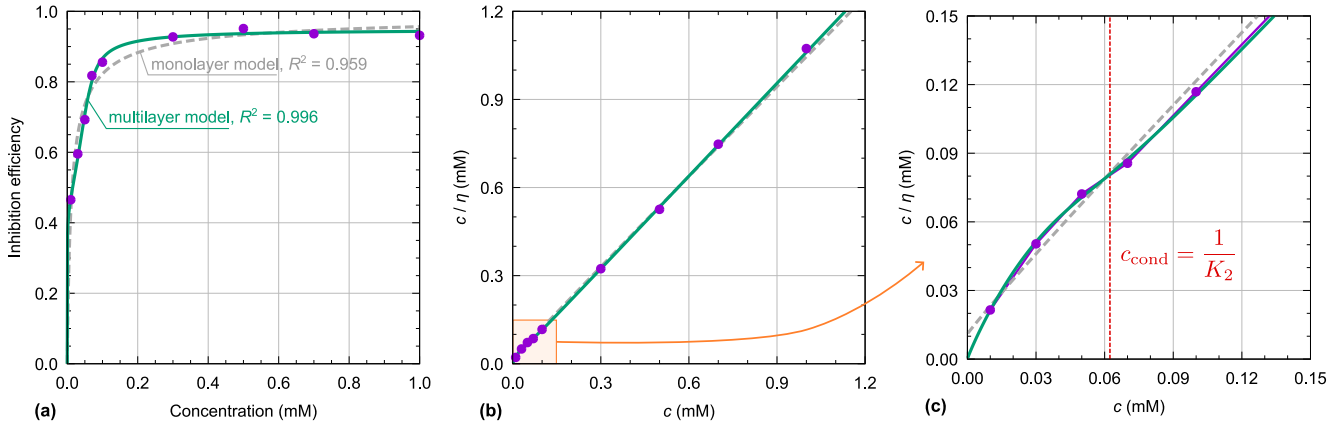

Fig. 11. POAMO-23 experimental data of Osman et al. [7] fitted with the monolayer model of Eq. (40) (gray dashed) and the BET-8 based multilayer model of Eq. (29) (green solid). (a) Inhibition efficiency as a function of concentration, and (b,c) the corresponding c/η versus c plots, with panel (c) focusing on low concentrations.

Furthermore, it was shown that multilayer adsorption reduces the slope of the c/η versus c curve relative to the monolayer case and gives rise to increased curvature at concentrations below the point at which the inhibitor condenses on the surface. While this multilayer-induced bending at low concentrations resembles that caused by other effects — such as repulsive lateral interactions, multisite adsorption, or surface heterogeneity [1] — the overall curvature resulting from multilayer adsorption is distinct. In particular, a hallmark of the multilayer curve is its bent, arching shape above the $c/\eta = c$ line for $c \lesssim c_{\mathrm{cond}}$, followed by a linear regime at higher concentrations. This characteristic curve shape appears to be supported by the analysis of the available experimental data, which exhibit the predicted hallmark of the multilayer curve, albeit with a rather shallow curvature, due to which the confirmation cannot be considered conclusive. Indeed, the analysis shows that under many conditions the curvature of the multilayer curve is inherently modest. On this basis, it is argued that in experiments where only a limited number of data points are sampled, these features are often not sufficiently distinctive to allow for the identification of multilayer behavior. This helps explain why the $\theta \approx \eta$ approximation — which implicitly assumes monolayer adsorption — has been so widely accepted and used.

Finally, the analyses presented here and in previous work [1] reveal a general trend: effects that increase surface coverage reduce the slope of c/θ versus c plots, whereas effects that lower surface coverage increase it. Although this conclusion appears self-evident from inspection of the c/θ expression itself, it is not always immediately recognized. Among the studied effects, attractive lateral interactions and multilayer adsorption result in slopes less than one on c/θ versus c plots—not to be confused with c/η versus c plots, which are often treated as if they were c/θ plots. In contrast, repulsive lateral interactions, multisite adsorption, and surface heterogeneities yield slopes greater than one.

Declaration of Generative AI and AI-assisted technologies in the writing process

The author used ChatGPT (developed by OpenAI) to assist with language editing. All content was created and reviewed by the author, who takes full responsibility for the integrity and accuracy of the manuscript.

Declaration of competing interest

The author declares that he has no known competing financial interests or personal relationships that could have appeared to influence the work reported in this paper.

Acknowledgments

This work has been financially supported by the Slovenian Research and Innovation Agency (Grant No. P2-0393).

Appendix A. Technical details

Graphs were plotted with the Gnuplot software [19] and their post-processing was done in `Inkscape` [20]. Gnuplot was also used for fitting. Derivation of equations was facilitated with WolframAlpha [21].

Appendix B. Derivation of the BET adsorption isotherm

The BET adsorption model [14] can be viewed as extension of the Langmuir adsorption model [13] that considers multilayer adsorption. This implies that Langmuir-like assumptions apply, apart from the monolayer constraint being released.

At the equilibrium, the surface area exclusively covered by i layers is constant. This implies that for the bare surface ($i = 0$), the rate of adsorption on the bare surface equals the rate of desorption from the first layer, which can be written as:

$$a_1 c S_0 = d_1 \exp\left(\frac{E_1^{\mathrm{ads}}}{RT}\right) S_1, \tag{B.1}$$

where a_1 and d_1 are the first-layer adsorption and desorption rate constants (mnemonic: $a \equiv$ adsorption, $d \equiv$ desorption), c is the molecular concentration in the bulk solution, E_1^{ads} is the molecular adsorption energy on the bare surface, R is the gas constant, and T is the temperature.

For the subsequent layers, as schematically illustrated in Fig. B.1, S_i can increase in two ways (by adsorption onto layer $i-1$ and by desorption from the layer i+1) and decrease in two ways (by adsorption onto the layer i and by desorption from the layer i). For example, for S_1 this implies:

$$a_1 c S_0 + d_2 \exp\left(\frac{E_2^{\mathrm{ads}}}{RT}\right) S_2 = a_2 c S_1 + d_1 \exp\left(\frac{E_1^{\mathrm{ads}}}{RT}\right) S_1, \tag{B.2}$$

where E_2^{ads} is the energy of adsorption onto the first layer, i.e., the adsorption energy for forming the second layer. By utilizing the equality of Eq. (B.1), we get:

$$d_2 \exp\left(\frac{E_2^{\mathrm{ads}}}{RT}\right) S_2 = a_2 c S_1. \tag{B.3}$$

Using the above arguments, it is straightforward to show that analogous relations hold also for further layers. Hence, we can generalize it as:

$$d_i \exp\left(\frac{E_i^{\text{ads}}}{RT}\right) S_i = a_i c S_{i-1}, \tag{B.4}$$

which after rearrangement gives:

$$S_i = c\frac{a_i}{d_i} \exp\left(-\frac{E_i^{\text{ads}}}{RT}\right) S_{i-1}. \tag{B.5}$$

By assuming that adsorption energy for forming layers beyond the first layer is the same for all of them and that the a_i/d_i ratios corresponding to that layers are also the same — i.e., $E_i^{\text{ads}} = E_2^{\text{ads}}$ and $a_i/d_i = a_2/d_2$ for $i \geq 2$ — we can write:

$$S_i = c\frac{a_2}{d_2} \exp\left(-\frac{E_2^{\text{ads}}}{RT}\right) S_{i-1} \qquad \text{for } i \geq 2. \tag{B.6}$$

By dividing both sides of this equation by S (cf. Eq. (2)), we get:

$$\theta_i = c\frac{a_2}{d_2} \exp\left(-\frac{E_2^{\text{ads}}}{RT}\right) \theta_{i-1} \qquad \text{for } i \geq 2. \tag{B.7}$$

Likewise, we get for θ_1 by rearranging Eq. (B.1):

$$\theta_1 = \underbrace{c\frac{a_1}{d_1} \exp\left(-\frac{E_1^{\text{ads}}}{RT}\right)}_{K_1} \theta_0. \tag{B.8}$$

Note that the underbraced $a_1/d_1 \exp(\cdots)$ term corresponds to the adsorption equilibrium constant for the formation of the first layer (K_1). To realize this, consider the first-layer adsorption reaction:

$$\text{Mol}_{(\text{sol})} + \square \rightleftharpoons \text{Mol}_{(\text{ad})}, \tag{B.9}$$

where $\text{Mol}_{(\text{sol})}$ stands for a molecule in the bulk solution, $\square$ for a free adsorption site, and $\text{Mol}_{(\text{ad})}$ for an adsorbed molecule. The adsorption equilibrium constant K_1 can be written as:

$$K_1 = \frac{[\text{Mol}_{(\text{ad})}]}{[\text{Mol}_{(\text{sol})}][\square]} = \frac{\theta_1}{c\theta_0}. \tag{B.10}$$

By expressing the $\theta_1/(c\theta_0)$ ratio with Eq. (B.8), we get:

$$K_1 = \frac{a_1}{d_1} \exp\left(-\frac{E_1^{\text{ads}}}{RT}\right). \tag{B.11}$$

Analogously for subsequent layers, we can write:[1]

$$K_2 = \frac{a_2}{d_2} \exp\left(-\frac{E_2^{\text{ads}}}{RT}\right). \tag{B.12}$$

By utilizing these definitions of K_1 and K_2, Eq. (B.7) can be rewritten as:

$$\theta_i = cK_2\theta_{i-1} = (cK_2)^i \frac{K_1}{K_2}\theta_0, \tag{B.13}$$

where for the second equality, θ_{i-1} was recursively expressed from the first equality until i was reduced to 1, and Eq. (B.8) was used to express θ_1. By making the following substitutions:

$$x = cK_2 \qquad \text{and} \qquad w = \frac{K_1}{K_2}, \tag{B.14}$$

[1] The adsorption equilibrium constant is related to the standard adsorption Gibbs energy via the well-known thermodynamic relation in Eq. (33) of the main text. By equating Eq. (B.11) or (B.12) with Eq. (33), it is straightforward to show that the relationship between the adsorption energy and the standard adsorption Gibbs energy is:
$\Delta G_{i,\text{ads}}^{\circ\,\text{plain}} = E_i^{\text{ads}} + RT \ln \frac{d_i}{a_i c^\circ}$,
where c° is the standard-state concentration of 1 M, used to make the quotient $\frac{d_i}{a_i c^\circ}$ dimensionless, and i refers to either 1 or 2. This equation implies that the entropic contributions to the standard adsorption Gibbs energy are implicitly included in the adsorption and desorption rate constants, a_i and d_i; recall that $G = E + pV - TS$.

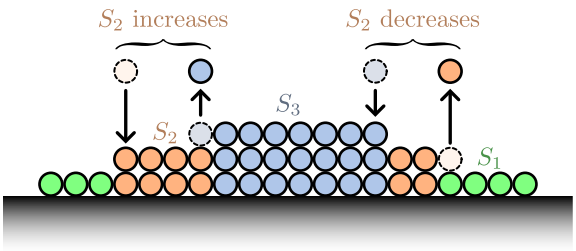

Fig. B.1. Schematic illustration of how S_2 can increase (by adsorption onto the first layer or desorption from the third layer) and decrease (by desorption from the second layer or adsorption onto it).

the equation for θ_i can be simplified to:

$$\theta_i = x^i w \theta_0. \tag{B.15}$$

Note that in the original BET derivation [14], the symbol c was used for the K_1/K_2 ratio. However, in the present work, c denotes concentration; therefore, the ratio is represented by w to avoid ambiguity.

We can solve Eq. (B.15) for θ_0 by noting, from Eqs. (1) and (2), that

$$\begin{aligned} 1 &= \sum_{i=0}^{\infty} \theta_i \\ &= \theta_0 + \sum_{i=1}^{\infty} \theta_i = \theta_0 + w\theta_0 \sum_{i=1}^{\infty} x^i \\ &= \theta_0 \left(1 + w\frac{x}{1-x}\right) \qquad \text{for } x < 1, \end{aligned} \tag{B.16}$$

where the $\sum_{i=1}^{\infty} x^i = x/(1-x)$ relation was used, which holds for $x < 1$. Hence:

$$\theta_0 = \frac{1-x}{1-x+wx} \qquad \text{for } x < 1. \tag{B.17}$$

Finally, the total molecular coverage (θ) can be expressed as:

$$\theta = \sum_{i=1}^{\infty} i\theta_i = w\theta_0 \sum_{i=1}^{\infty} i x^i = w\theta_0 \frac{x}{(1-x)^2} \qquad \text{for } x < 1. \tag{B.18}$$

Substituting the expression for θ_0 from Eq. (B.17) gives:

$$\theta = \frac{wx}{(1-x)(1-x+wx)}, \tag{B.19}$$

which is the BET isotherm. By inserting the definitions of x and w from Eq. (B.14), we obtain:

$$\theta = \frac{cK_1}{(1-cK_2)(1-cK_2+cK_1)}. \tag{B.20}$$

Note that this equation diverges at $cK_2 = 1$, i.e., the coverage becomes infinite at the concentration $c = K_2^{-1}$. Physically, this corresponds to the condensation of the adsorbate on the surface. Indeed, the BET derivation relies on the condition $x < 1$, which implies $cK_2 < 1$.

Appendix C. The BET-*n* adsorption isotherm

If, for some reason, the adsorbate can form up to only n layers, then the summations in Eqs. (B.16) and (B.18) should be evaluated only up to n terms [17]. In this case, Eq. (B.16) becomes:

$$1 = \sum_{i=0}^{n} \theta_i = \theta_0 \left(1 + w\frac{x(1-x^n)}{1-x}\right), \tag{C.1}$$

hence:

$$\theta_0 = \left(1 + w\frac{x(1-x^n)}{1-x}\right)^{-1} \equiv \theta_0(n), \tag{C.2}$$

where the notation $\theta_0(n)$ is used to indicate the n-dependence explicitly and to distinguish it from θ_0 in the standard BET model. The expression

for coverage of Eq. (B.19) thus transforms to:

$$\theta(n) = \frac{wx\left(1-(n+1)x^n+nx^{n+1}\right)}{(1-x)\left(1+(w-1)x-wx^{n+1}\right)}. \tag{C.3}$$

This equation is referred to as the BET-n isotherm in the main text, where the suffix n indicates the maximum number of layers the adsorbate can form. Indeed, it is easy to verify that:

$$\lim_{x\to\infty}\theta(n) = n. \tag{C.4}$$

Furthermore, note that the BET-n isotherm reduces to the BET isotherm of Eq. (B.19) for $n \to \infty$ and $x < 1$.

It is worth noting that, for the BET-n isotherm, the condition $x < 1$ is not required, as the BET-n expression does not diverge at $x = 1$, which corresponds to the concentration $c = K_2^{-1}$. It can be shown that at this concentration, the BET-n coverage is:

$$\theta(n) = \frac{nw(1+n)}{2(1+nw)} \qquad \text{at } x = 1 \text{ or } c = \frac{1}{K_2}. \tag{C.5}$$

Appendix D. Supplementary data

Supplementary material related to this article can be found online at https://doi.org/10.1016/j.corsci.2025.113323.

Data availability

The data presented in the manuscript are contained within it, while the scripts used for fitting and generating the plots are available upon request.

References

[1] A. Kokalj, On the use of the Langmuir and other adsorption isotherms in corrosion inhibition, Corros. Sci. 217 (2023) 111112, http://dx.doi.org/10.1016/j.corsci.2023.111112.

[2] A. Kokalj, A general-purpose adsorption isotherm for improved estimation of standard adsorption free energy, Corros. Sci. 217 (2023) 111124, http://dx.doi.org/10.1016/j.corsci.2023.111124.

[3] A. Kokalj, On the estimation of standard adsorption free energy from corrosion inhibition efficiencies, Corros. Sci. 217 (2023) 111139, http://dx.doi.org/10.1016/j.corsci.2023.111139.

[4] M.S. Walczak, P. Morales-Gil, R. Lindsay, Determining Gibbs energies of adsorption from corrosion inhibition efficiencies: Is it a reliable approach? Corros. Sci. 155 (2019) 182–185, http://dx.doi.org/10.1016/j.corsci.2019.04.040.

[5] W. Xing, Y. Shan, D. Guo, T. Lu, S. Xi, Mechanism of iron inhibition by stearic acid Langmuir–Blodgett monolayers, Corrosion 51 (1) (1995) 45–49, http://dx.doi.org/10.5006/1.3293576.

[6] M.L. Free, Understanding the effect of surfactant aggregation on corrosion inhibition of mild steel in acidic medium, Corros. Sci. 44 (12) (2002) 2865–2870, http://dx.doi.org/10.1016/S0010-938X(02)00080-X.

[7] M.M. Osman, R.A. El-Ghazawy, A.M. Al-Sabagh, Corrosion inhibitor of some surfactants derived from maleic-oleic acid adduct on mild steel in 1 M H_2SO_4, Mater. Chem. Phys. 80 (1) (2003) 55–62, http://dx.doi.org/10.1016/S0254-0584(01)00588-0.

[8] D.K. Kozlica, A. Kokalj, I. Milošev, Synergistic effect of 2-mercaptobenzimidazole and octylphosphonic acid as corrosion inhibitors for copper and aluminium – An electrochemical, XPS, FTIR and DFT study, Corros. Sci. 182 (2021) 109082, http://dx.doi.org/10.1016/j.corsci.2020.109082.

[9] E. Vernack, S. Zanna, A. Seyeux, D. Costa, F. Chiter, P. Tingaut, P. Marcus, ToF-SIMS, XPS and DFT study of the adsorption of 2-mercaptobenzothiazole on copper in neutral aqueous solution and corrosion protection in chloride solution, Corros. Sci. 210 (2023) 110854, http://dx.doi.org/10.1016/j.corsci.2022.110854.

[10] S. Sharma, X. Ko, Y. Kurapati, H. Singh, S. Nešić, Adsorption behavior of organic corrosion inhibitors on metal surfaces—Some new insights from molecular simulations, Corrosion 75 (2018) 90–105, http://dx.doi.org/10.5006/2976.

[11] Y. Duda, R. Govea-Rueda, M. Galicia, H.I. Beltrán, L.S. Zamudio-Rivera, Corrosion inhibitors: Design, performance, and computer simulations, J. Phys. Chem. B 109 (47) (2005) 22674–22684, http://dx.doi.org/10.1021/jp0522765.

[12] A. Kokalj, Considering the concept of synergism in corrosion inhibition, Corros. Sci. 212 (2023) 110922, http://dx.doi.org/10.1016/j.corsci.2022.110922.

[13] I. Langmuir, The adsorption of gases on plane surfaces of glass, mica and platinum, J. Am. Chem. Soc. 40 (9) (1918) 1361–1403, http://dx.doi.org/10.1021/ja02242a004.

[14] S. Brunauer, P.H. Emmett, E. Teller, Adsorption of gases in multimolecular layers, J. Am. Chem. Soc. 60 (2) (1938) 309–319, http://dx.doi.org/10.1021/ja01269a023.

[15] A. Kokalj, D. Costa, Model study of penetration of Cl^- ions from solution into organic self-assembled-monolayer on metal substrate: Trends and modeling aspects, J. Electrochem. Soc. 168 (7) (2021) 071508, http://dx.doi.org/10.1149/1945-7111/ac0a24.

[16] F. Chiter, D. Costa, M. Poberžnik, I. Milošev, P. Marcus, A. Kokalj, DFT study of Cl^- ingress into organic self-assembled monolayers on aluminum, J. Electrochem. Soc. 170 (7) (2023) 071504, http://dx.doi.org/10.1149/1945-7111/ace334.

[17] A. Ebadi, J.S. Soltan Mohammadzadeh, A. Khudiev, What is the correct form of BET isotherm for modeling liquid phase adsorption? Adsorption 15 (1) (2009) 65–73, http://dx.doi.org/10.1007/s10450-009-9151-3.

[18] A. Kokalj, Corrosion inhibitors: physisorbed or chemisorbed? Corros. Sci. 196 (2022) 109939, http://dx.doi.org/10.1016/j.corsci.2021.109939.

[19] T. Williams, C. Kelley, et al., Gnuplot 5.4, 2020, http://www.gnuplot.info/.

[20] Inkscape Project, Inkscape, version 1.0.2, 2021, https://inkscape.org.

[21] Wolfram Research, Inc., Wolfram|alpha: Computational intelligence, 2025, Online. https://www.wolframalpha.com. (Last Accessed 31 July 2025).